

# AirCode: A Robust Object Encoding Method

Kuan Xu<sup>1</sup>, Chen Wang<sup>†2</sup>, Chao Chen<sup>1</sup>, Wei Wu<sup>1</sup>, and Sebastian Scherer<sup>2</sup>

**Abstract**—Object encoding and identification is crucial for many robotic tasks such as autonomous exploration and semantic relocalization. Existing works heavily rely on the tracking of detected objects but have difficulty to recall revisited objects precisely. In this paper, we propose a novel object encoding method, which is named as AirCode, based on a graph of key-points. To be robust to the number of key-points detected, we propose a feature sparse encoding and object dense encoding method to ensure that each key-point can only affect a small part of the object descriptors, leading it to be robust to viewpoint changes, scaling, occlusion, and even object deformation. In the experiments, we show that it achieves superior performance for object identification than the state-of-the-art algorithms and is able to provide reliable semantic relocalization. It is a plug-and-play module and we expect that it will play an important role in various applications.

## I. INTRODUCTION

Object encoding and identification is of great importance for many robotic tasks such as autonomous exploration and semantic re-localization in simultaneous localization and mapping (SLAM). For example, in autonomous exploration, an efficient and robust object encoding benefits the decision process when a robot revisits a specific landmark object [1]. Without the capability of object matching, a semantic SLAM system may easily drift and subsequently lead to an unreliable localization [2]. However, existing object encoding methods easily produce false matches due to viewpoint or scaling changes, hence a robust and efficient object encoding method is necessary for many robotic applications.

To save computational resources, object matching in SLAM is often based on key-point features [3], as the feature-based SLAM methods [4] are still widely used. Inspired by the recent progresses in deep learning-based key-point detector [5] and feature matching methods [6], it becomes intuitive to encode an object via a group of key-points in an end-to-end manner, where the key-points on the same object form a graph neural network. Therefore, we can take the graph embeddings as the object descriptors.

However, this is not straightforward and very difficult, since the number of detected object key-points are affected by many factors such as illumination and object deformation. Moreover, during robot exploration, robots often observe part of the objects due to occlusion and different viewpoints, resulting in that the object key-points only have a small overlap across

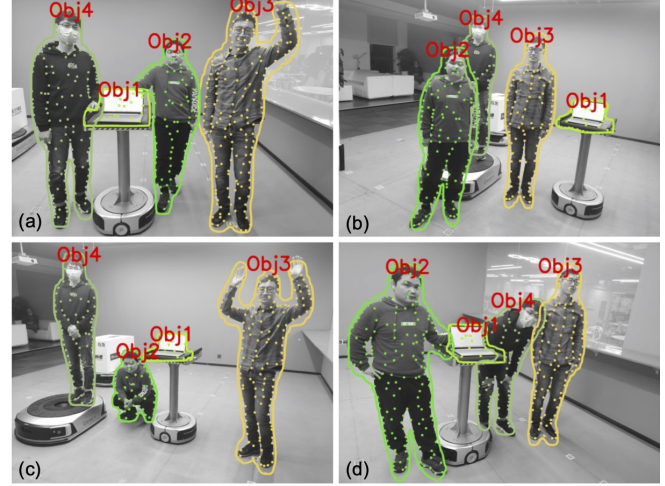


Fig. 1: An object matching example. Four objects including 1 rigid object (laptop) and 3 non-rigid objects (human) are identified. Our encoding method is insensitive to viewpoint (Obj 1 in (b) and (d)), scaling (Obj 3 and Obj 4), occlusion (Obj 4), and even posture change (Obj 2 and Obj 3).

different frames. Therefore, the key-points graph embedding will be easily affected, which makes it difficult to directly apply a graph network [7]. To solve this problem, we argue that a key-point descriptor should have a sparse effect on the object embedding. This means that only a few positions of an object descriptor can be affected if a key-point is added or removed from an object graph. To achieve this, we propose a sparse object encoding method, which is robust to the change of viewpoint and object deformation.

In summary, the main contributions of this paper are

- We introduce a simple yet effective pipeline, AirCode, for robust object encoding and present a plug-and-play sparsity layer to cluster similar key-points.
- We propose a sparse loss for key-point features and a dense loss for object features to ensure the object encoder to be insensitive to specific feature points.
- AirCode provides reliable object matching as shown in Fig. 1 and we demonstrate its effectiveness in semantic relocalization compared to the state-of-the-art methods.

## II. RELATED WORK

We will review both object encoding and visual place recognition methods, since some place recognition algorithms can also be applied to object matching. General detection networks such as Mask R-CNN [8] will not be included, since they are difficult to be used for object matching.

<sup>†</sup>Corresponding Author. Source codes and pre-trained models are available at <https://github.com/wang-chen/AirCode>.

<sup>1</sup>Kuan Xu, Chao Chen, and Wei Wu are with the Geek+ Corp. E-mail: {xukuan, chenchao, merlinwu}@geekplus.com

<sup>2</sup>Chen Wang and Sebastian Scherer are with the Robotics Institute, Carnegie Mellon University, Pittsburgh, PA 15213, USA. E-mail: chenwang@dr.com; basti@andrew.cmu.edu

### A. Handcrafted Feature-based Methods

Fast appearance-based mapping (FABMAP) [9] is one of the most classic approaches on handcrafted features. The authors train a visual vocabulary of SURF feature [10] using hierarchical k-means clustering to discretize the high dimensional representation, and then the offline trained visual vocabulary can be used to match features to identify revisited objects. Furthermore, DBoW2 [11] follows this idea and employs ORB binary descriptor [12] to achieve a faster speed. In [13], dynamic island algorithm is proposed to maintain the vocabulary by grouping similar images, in which repetitive registration of same descriptor across multiple frames is able to be identified. The strategy of removing redundant descriptors can keep the database at a small scale.

Schlegel *et al.* [14] introduce an online trained Hamming distance embedded binary search tree (HBST) for image retrieval, which is much faster than traditional FLANN matching methods. However, due to the use of raw descriptors to build the incremental visual vocabulary tree, its memory cost is huge. Reducing the dimension of local features is also an alternative solution. Inspired by the image encoding methods, Carrasco *et al.* [15] apply hash coding to the local features array, which makes the features extracted from single image more compact. Gehrig *et al.* [16] reduce the dimension of BRISK [17] feature with principle component analysis (PCA). They directly employ k-nearest neighbor (K-NN) search on projected descriptors, which makes the query speed several milliseconds faster than searching on pre-trained visual vocabulary. However, those methods are all based on handcrafted feature extraction, which is not robust enough when the environment is changed.

Tsintotas *et al.* [18] adopt a dynamic quantization strategy to train the feature online, in which a growing neural gas [19] network is applied. To utilize both structural and visual information, Stumm *et al.* introduce covisibility graph to represent visual observations [20]. To jointly consider external information, Schlegel *et al.* embed continuous and selector cues by augmenting each feature descriptor with a binary string [21]. The feature-based methods performs not well when the descriptors are not discriminative enough, hence we argue that an object-level place recognition is necessary.

### B. Deep Feature-based Methods

Convolutional neural network (CNN) has made great progress in many computer vision tasks and this triggers another research trend [22]. For example, Z. Chen *et al.* [23] introduce a multi-scale feature encoding method, in which two CNN architectures are trained and generate features. The viewpoint invariant features provide a huge performance boost. Relja *et al.* propose NetVLAD [24], in which the authors train a convolutional neural network to replace the parameters of vector of locally aggregated descriptors (VLAD). Instead of relying on a single method, Hausler *et al.* [25] combine multiple methods of image processing for visual place recognition, including sum of absolute difference, histogram of oriented gradients (HOG) [26], CNN spatial Max pooling, and CNN spatial Arg-Max pooling.

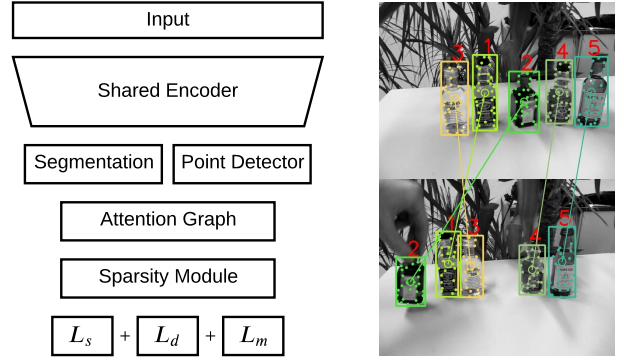


Fig. 2: The network structure of our object encoding method and an example of object matching from the OTB dataset.

To overcome the problem of training data deficiency and multi-modality input dissimilarity, an RGB-D object recognition framework is proposed to effectively embed depth and point cloud data into the RGB domain [27]. Zaki *et al.* incorporate depth information into a transferred CNN model from image recognition by rendering objects from a canonical perspective and colorizing the depth channel according to distance from the object center [28]. HP-CNN [29] presents a multi-scale object feature representation based on a multi-view 3D object pose using RGB-D sensors.

Our object encoding method is established on deep feature points and descriptors, which has received increasing attentions recently. For example, SuperPoint [5] proposes a self-supervised framework for training interest point detectors and descriptors. SuperGlue [6] introduces a graph attention model for feature matching. Intuitively, the interest points and their descriptors form a large temporal growing graph, in which the feature points are nodes, and their associated descriptors are the node features.

## III. METHODOLOGY

### A. Formulation

Given  $M$  key-points from the same object, each point is denoted as a position  $\mathbf{p}_i = (x, y)$  and its associated descriptor  $\mathbf{d}_i \in \mathbb{R}^{N_p}$ , where  $i \in [1, M]$  and  $N_p$  is the dimension of the point descriptor. Our goal is to design a graph neural network to generate an object descriptor  $\mathbf{D}_k \in \mathbb{R}^{N_o}$  for robust object matching based on the key-points, where  $N_o > N_p$  is the dimension of the object descriptor. To this end, we propose a simple yet effective pipeline shown in Fig. 2. Each object is taken as a graph, where the nodes are the points  $\{\mathbf{p}_i\}$  with descriptors  $\{\mathbf{d}_i\}$  and the edges are point connections. In the experiments, the points and their descriptors are obtained from point detector SuperPoint [5] and object segmentation masks from Mask R-CNN [8]. However, they can also be obtained from handcrafted descriptors such as SIFT [30].

In the pipeline shown in Fig. 2, we use the off-the-shelf network modules including segmentation (Mask R-CNN), point detector (SuperPoint), and attention graph (GAT [31]). Specifically, Mask R-CNN and SuperPoint have a shared

backbone encoder VGG-16 [32]. For simplicity, we skip their details and mainly present our sparsity embedding module.

### B. Graph Embedding with Sparse Node Features

1) *Motivation*: Inspired by the fact that human can easily identify an object by recognizing both local distinctive features and global structure [33], we believe that a robust object encoding method should have the following properties: (I) An object descriptor should be able to encode both the local key-point features and the global structural information; (II) To be insensitive to viewpoint changes and object deformation, the object descriptor should not be significantly affected when a few number of key-points are added or removed.

Therefore, we argue that if only specific positions of the object descriptor can be affected by a key-point (in other words, a key-point has a sparse effect on its object descriptor), then we will be able to obtain a viewpoint invariant object encoding method. This inspires us to formulate the object encoding as a problem of graph sparse embedding.

2) *Node Encoding*: To encode the local pattern and global structural information simultaneously, we take the concatenation of point features and their positions as the node embedding. Assume a node embedding is  $\mathbf{x}_i^{(1)}$ , then

$$\mathbf{x}_i^{(1)} = [\mathbf{d}_i || \text{MLP}(\mathbf{p}_i)], \quad \mathbf{x}_i \in \mathbb{R}^{N_n}, \quad (1)$$

where  $N_n = N_p + N_m$ ,  $||$  is the concatenation operator,  $\text{MLP}: \mathbb{R}^2 \mapsto \mathbb{R}^{N_m}$  is a multi-layer perceptron module, and the superscript of  $\mathbf{x}_i^{(l)}$  denotes the  $l$ -th layer. In practice, the position  $\mathbf{p}_i$  is normalized to  $[-1, 1]$  by its object size, which takes the object center as the origin. This encodes the object structure into the node embedding, which will be helpful for learning the sparse non-zero locations shown below.

3) *Sparsity Layer*: Inspired by the (II) property mentioned in Section III-B.1, which means that a key-point feature should only be able to affect the object descriptor on sparse locations, so that the key-points can be added or removed without significantly changing the object descriptor. Moreover, to fully utilize the expressive power of the object descriptor, key-points with different local patterns should be written into distinctive locations. Therefore, the sparse locations should be learned from the contents of the node embeddings. To achieve this, we define two branches for the sparsity layer in (2) for the location and content features, respectively.

$$^{(l+1)}\mathbf{x}_i^L = \text{ReLU}(\mathbf{W}_L^{(l)} \cdot ^{(l)}\mathbf{x}_i^L), \quad (2a)$$

$$^{(l+1)}\mathbf{x}_i^C = \text{ReLU}(\mathbf{W}_C^{(l)} \cdot ^{(l)}\mathbf{x}_i^C), \quad (2b)$$

where  $\mathbf{W}_L^{(l)}, \mathbf{W}_C^{(l)} \in \mathbb{R}^{N_o \times N_n^l}$ ,  $N_n^l < N_o$  are the learnable location and content weights, respectively. We set the input of (2) as the same, i.e.,  $^{(1)}\mathbf{x}_i^L = ^{(1)}\mathbf{x}_i^C$ , which is also the output of the attention graph. Specifically, each of the two branches has two layers to learn the location and content features, respectively.

Intuitively, if the location feature  $\mathbf{x}_i^L$  is a sparse vector that only a few locations are non-zeros, an object descriptor  $\mathbf{D}_k$  in (3) will be insensitive to the change of key-points.

$$\mathbf{D}_k = \frac{\mathbf{W}_o}{M} \sum_{i=1}^M \mathbf{x}_i^L \odot \mathbf{x}_i^C, \quad (3)$$

where  $\mathbf{W}_o$  is learnable parameters and the operator  $\odot$  is an element-wise multiplication. Note that the summation in (3) is a symmetric operator, which is able to ensure the object descriptor  $\mathbf{D}_k$  to be invariant to the permutation of key-points.

It is intuitive that fewer number of non-zeros in the location feature  $\mathbf{x}_i^L$  means that the object descriptor  $\mathbf{D}_k$  will be less affected by the key-point  $i$ . We next show that how can we ensure the sparsity of the location feature  $\mathbf{x}_i^L$ .

4) *Sparse Location Loss*: We define the location sparse loss  $L_s$  as the  $\ell_1$ -norm of  $\mathbf{x}_i^L$  to promote the sparsity:

$$L_s := \sum_{i=1}^M \|\phi(\mathbf{x}_i^L)\|_1, \quad (4)$$

where  $\phi(\mathbf{x}) = \mathbf{x}/\|\mathbf{x}\|_2$  is a  $\ell_2$ -normalization function, which is to prevent the location feature from being zero. The  $\ell_1$  loss for promoting vector sparsity has been widely used in sparse coding for dictionary learning [34]. An intuitive geometric explanation in 2-D space is that the points located on the intersection of axes and unit circle has the minimum  $\ell_1$ -norm, which means that some coordinates tend to be zero.

5) *Dense Feature Loss*: The location sparse loss ensures that the key-point descriptors are encoded into sparse locations on the object descriptor. On the other hand, we also expect that distinctive key-point features are able to cover different locations, which can maximize the space utilization rate of the object descriptor, otherwise the location weights  $\mathbf{W}_L$  will simply learn to map all key-points to the same sparse locations, which is not expected. Therefore, we define a feature dense loss  $L_d$  as the negative  $\ell_1$ -norm of the summed location features to improve the density of the object descriptor.

$$L_d := \max \left( 0, \delta - \phi \left( \left\| \sum_{i=1}^M \mathbf{x}_i^L \right\|_1 \right) \right), \quad (5)$$

where  $\delta > 0$  is a positive constant. A major difference of the dense loss (5) from the sparse loss (4) is that the summation operator is inside of the  $\ell_1$ -norm, while the  $\ell_2$ -normalization function  $\phi$  is outside of the  $\ell_1$ -norm. This is because that the object descriptor (3) is an element-wise summation of the key-point features. Intuitively, by optimizing the sparse loss and dense loss simultaneously, we are able to push the key-point location features to be sparse, while retaining the density of object descriptor, so that similar key-points will share similar locations, while distinctive key-points tend to cover different locations. This means that the object descriptor will be insensitive to the changes of key-points, resulting in the invariance to viewpoint changes and object deformation.

Note that the sparsity in this paper is different from the traditional sparse coding techniques [34] and deep sparse coding network [35] which are to learn a dictionary and minimize a reconstruction error, while ours is to learn sparse key-point features without any approximation and dictionary. It is also different from the model compression networks such as [36] to learn sparse convolutional weights, as we have no sparse constraints on the learnable weights  $\mathbf{W}_L$ .



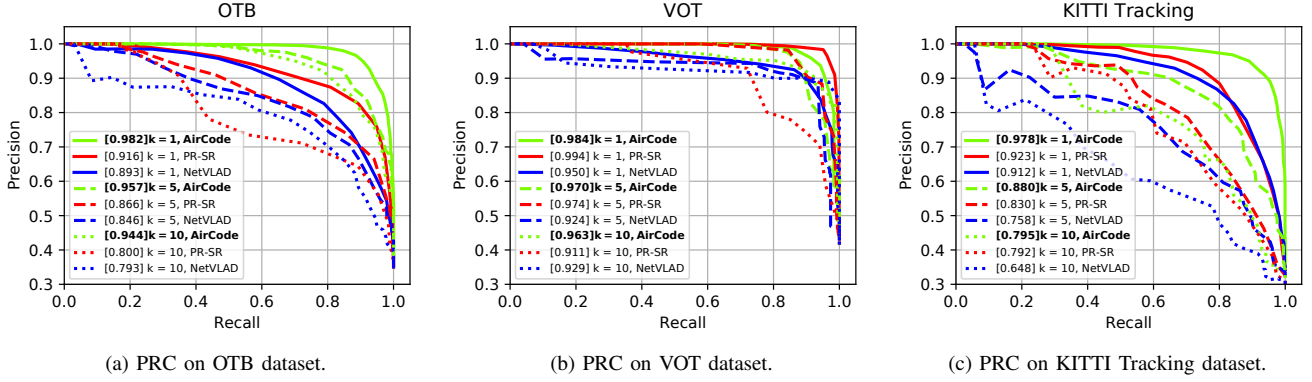


Fig. 3: The precision-recall curves (PRC) on object matching. The area under curves are shown in the [brackets].

6) *Object Matching Loss*: The object matching loss  $L_m$  maximizes the cosine similarity for positive object pairs, while minimizes the cosine similarity for negative pairs.

$$L_m := \sum_{\{p,q\} \in P^+} (1 - S(\mathbf{D}_p, \mathbf{D}_q)) + \sum_{\{p,q\} \in P^-} \max(0, S(\mathbf{D}_p, \mathbf{D}_q) - \zeta),$$

where  $\zeta = 0.2$  is a constant margin,  $S$  is the cosine similarity, and  $P^+/P^-$  are positive/negative object pairs, respectively.

#### IV. EXPERIMENTS

##### A. Implementation Details and Baseline

We take pre-trained backbone CNN and key-point detector from SuperPoint [5], pre-trained segmentation header from Mask R-CNN [8], and finetune the entire network on COCO dataset [37]. Random homographies are generated for data augmentation, including the perspective, translation, rotation, and scale transforms. We take a batch size of 16, a learning rate of  $10^{-5}$ , and the RMSprop [38] optimizer for training. In the experiments, we set  $N_p = 256$ ,  $N_m = 16$ , and  $N_o = 2048$ .

We note that an attention graph is also used in SuperGlue [6] to match feature points. It broadcasts node features from two images for point matching, while object embedding in our work is self-representative thus the node features can only be propagated within the object. Therefore, we don't take the point features from SuperGlue as our inputs, since we expect that an object descriptor doesn't use information from external images, so that one query descriptor can be matched to objects in database without exchanging information.

We perform extensive comparison with the state-of-the-art methods including NetVLAD [24] and PR-SR [2]. Specifically, NetVLAD is also a plug-and-play module and one of the most famous image matching methods. It has been adopted by many place recognition algorithms, e.g., [39], [40], which verifies its generalization ability. PR-SR applied a saliency detection technique to segment objects, which sometimes is not able to detect all objects. For fair comparison, we provide the ground truth mask of object segmentation for PR-SR and only compare with its object matching performance.

TABLE I: Object Matching on the OTB dataset.

	Method	Precision	Recall	F1
$k = 1$	NetVLAD	78.5	83.0	80.7
	PR-SR	82.7	89.3	85.9
	AirCode	<b>92.7</b>	<b>92.6</b>	<b>92.6</b>
$k = 3$	NetVLAD	72.7	79.7	76.0
	PR-SR	81.7	79.1	80.4
	AirCode	<b>88.0</b>	<b>85.3</b>	<b>86.6</b>
$k = 5$	NetVLAD	74.0	81.0	77.3
	PR-SR	81.0	73.2	76.9
	AirCode	<b>87.0</b>	<b>87.9</b>	<b>87.4</b>
$k = 10$	NetVLAD	70.2	80.7	75.1
	PR-SR	71.1	72.2	71.6
	AirCode	<b>85.2</b>	<b>86.9</b>	<b>86.0</b>

##### B. Object Matching

We first present the performance of the proposed method on object matching. Three datasets will be tested extensively, including OTB-2013 [41], VOT-2016 [42], and KITTI Tracking [43]. Note that we present performance on tracking datasets but don't compare with tracking methods such as [44], as they mainly use the information from consecutive frames, while we extract object descriptors for matching with any frames. Note that we don't perform finetuning on these datasets.

1) *OTB Dataset*: We select all sequences of OTB in which objects have labels in the COCO dataset and can be detected by more than 5 key-points. To test the robustness, we report the matching performance for frame pairs that has  $k-1$  ( $k > 1$ ) frames in between. Intuitively, matching is more difficult for larger  $k$  and object tracking is the case of  $k = 1$ . We take an object pair as a match if their cosine similarity is larger than a threshold  $\delta$ . The overall performance of precision, recall, and F1-score is presented in Table I. It can be seen that AirCode outperforms NetVLAD with a large margin of 5%-15% and outperforms PR-SR by a margin of 3%-10%. Intuitively, we can obtain the precision-recall curves (PRC) for each sequence by changing the threshold  $\delta$ . We report the precision-recall curves in Fig. 3a, in which the areas under curves (PRC) are reported in the brackets. AirCode achieves a much higher performance for all cases, i.e., an



Fig. 4: The examples of car matching in the KITTI Odometry dataset. Although all the cars look similar, AirCode is still able to correctly identify the same cars from different viewpoint.

TABLE II: Object Matching on the VOT dataset.

	Method	Precision	Recall	F1
$k = 1$	NetVLAD	90.9	88.7	89.8
	PR-SR	<b>98.3</b>	<b>95.1</b>	<b>96.7</b>
	AirCode	96.0	91.3	93.6
$k = 3$	NetVLAD	90.0	92.1	91.0
	PR-SR	<b>97.2</b>	<b>94.2</b>	<b>95.7</b>
	AirCode	94.0	89.2	91.5
$k = 5$	NetVLAD	89.5	90.4	89.9
	PR-SR	90.3	<b>90.4</b>	<b>90.3</b>
	AirCode	<b>90.9</b>	89.4	90.1
$k = 10$	NetVLAD	90.0	<b>90.5</b>	90.2
	PR-SR	77.9	85.1	81.3
	AirCode	<b>92.5</b>	89.1	<b>90.8</b>

TABLE III: Object Matching on the KITTI Tracking dataset.

	Method	Precision	Recall	F1
$k = 1$	NetVLAD	82.6	84.4	83.5
	PR-SR	82.0	84.3	83.1
	AirCode	<b>92.5</b>	<b>91.8</b>	<b>92.1</b>
$k = 3$	NetVLAD	72.7	74.1	73.4
	PR-SR	79.4	74.5	76.9
	AirCode	<b>86.5</b>	<b>83.4</b>	<b>84.9</b>
$k = 5$	NetVLAD	68.6	68.8	68.7
	PR-SR	78.5	70.4	74.2
	AirCode	<b>81.5</b>	<b>80.1</b>	<b>80.8</b>
$k = 10$	NetVLAD	57.4	65.3	61.1
	PR-SR	71.4	69.3	70.3
	AirCode	<b>73.7</b>	<b>72.7</b>	<b>73.2</b>

average higher performance of 8.9%, 11.1%, and 15.1% than NetVLAD and 6.6%, 9.1%, and 14.4% than PR-SR for  $k = 1$ , 5, and 10, respectively. We notice that the performance of AirCode decreases much slower with increasing  $k$  than other methods, which verifies its robustness.

2) *VOT Dataset*: The VOT dataset mainly contains blur and non-rigid objects such as human. The overall performance is presented in Table II, in which we achieve a higher performance of 1-5% than NetVLAD and comparable performance with PR-SR. The PRC performance is reported in Fig. 3b, in which we achieve a higher performance of 3.4%, 4.6%, and 3.4%, for  $k = 1$ , 5, and 10 than NetVLAD, respectively. Although PR-SR is better in some cases, we have a higher performance of 5.2% than PR-SR for  $k = 10$ , which means that AirCode is more robust to large viewpoint changes.

3) *KITTI Tracking Dataset*: The KITTI Tracking benchmark is a multi-object tracking dataset [43], thus we calculate the similarity of all object pairs in each frame pairs. The overall performance on precision, recall, and F1-score are reported in Table III in which we still achieve the best

performance. Their PRC are shown in Fig. 3c, in which we achieve a higher performance of 6.6%, 12.2%, and 14.7% than NetVLAD and 5.5%, 5.0%, and 0.3% than PR-SR for  $k = 1$ , 5, and 10, respectively.

### C. Semantic Relocalization

To further verify its robustness, we apply the proposed method to semantic relocalization, which will be evaluated on the KITTI Odometry dataset [45]. We select the sequences with significant loop closures, i.e., '00', '05', and '06'. We mainly re-identify cars for relocalization, which is much more difficult than matching distinct objects. Although the overall performance of relocalization will be slightly harmed, such setting is able to verify the robustness of the object descriptor, as the cars on the road in KITTI datasets are very similar thus the performance on car matching is more convincing.

The overall performance is listed in Table IV, in which we can see that we achieve more reliable performance than NetVLAD for all sequences. Note that we don't perform assistant techniques such as geometric verification [2] to

TABLE IV: Semantic Relocalization on KITTI Odoemtry.

Sequence	Method	Precision	Recall	F1
00	NetVLAD	21.1	41.3	27.9
	AirCode	<b>50.8</b>	<b>86.9</b>	<b>64.1</b>
05	NetVLAD	19.0	25.3	21.7
	AirCode	<b>43.7</b>	<b>48.0</b>	<b>45.7</b>
06	NetVLAD	39.0	27.4	32.2
	AirCode	<b>71.4</b>	<b>63.2</b>	<b>67.1</b>

ensure that the improvements coming from the proposed object descriptor. We also present the recall curves in Fig. 5, in which we accept the top  $N$  pairs as a re-localization. It can be seen that,  $\forall N, N \in [1, 20]$ , we are able to achieve better performance with a large margin than NetVLAD for all sequences, which verifies the effectiveness of AirCode. We don't employ PR-SR in this task, since it computes correlation for all object pairs, which is quite computationally heavy.

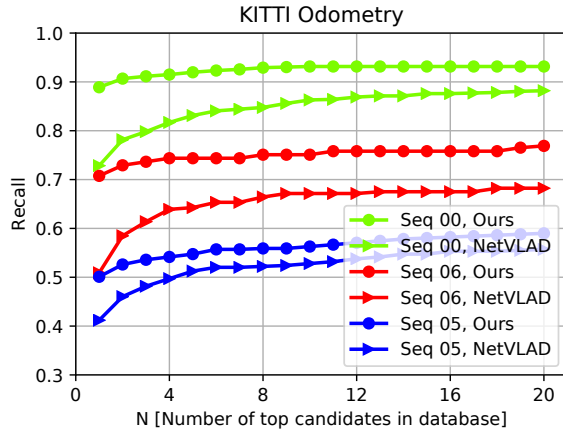
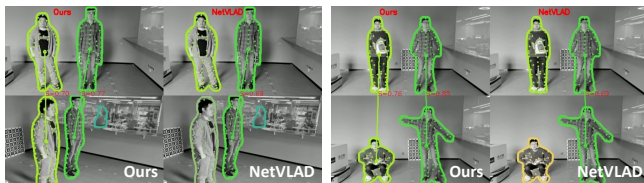


Fig. 5: The performance of semantic re-localization.

#### D. Live Demo & Limitation

In this section, we present a live demo to demonstrate the generalization ability and robustness of the proposed method. In this demo, we still use the pre-trained model mentioned in Section IV-B without any finetuning. It can be seen that AirCode is quite robust to the change of viewpoint in Fig. 6a and object deformation in Fig. 6b. For better visualization, it is suggested to watch the [video](#) attached to this paper.

One limitation of AirCode is that its robustness depends on the performance of object segmentation, thus the matching may not be stable when objects are not segmented correctly.

Fig. 6: The live object matching demo. Better to [Watch Video](#).

## V. PERFORMANCE ANALYSIS

### A. Sparsity Analysis

We provide the sparsity analysis for the proposed method based on COCO dataset [37]. The distribution of non-zero locations of the key-point features is shown in Fig. 7a, in which we can see that only 700-800 out of 2048 locations are non-zeros. This verifies the objective of sparse loss in (4). The statistics of non-zero locations of the object descriptor is presented in Fig. 7b. As expected, the non-zero locations increase with the number of key-point detected in the object, which also verifies the objective of dense loss (5). Note that we expect to group similar key-points into similar locations as in (2a), thus the space of object descriptor will not be quickly used up by increasing the number of key-points.

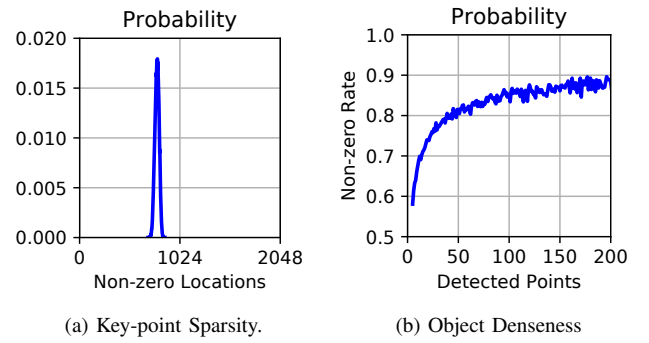


Fig. 7: The statistics of feature sparsity.

### B. Efficiency

This section presents the runtime of the proposed modules, which are listed in Table V. It can be seen that the sparsity layer only takes about 1 ms, which is much lower than the graph attention network used in this module. The overall running time is about 9.3 ms, which satisfies the real-time requirements of most robotic applications.

TABLE V: Runtime Analysis.

Module	Node Encoding	Graph	Sparsity	Overall
Time	0.847 ms	7.302 ms	1.131 ms	9.280 ms

## VI. CONCLUSION

In this paper, we present a novel object encoding method, which can be used in many robotic tasks such as autonomous exploration and semantic relocalization. It is a plug-and-play module and can be easily adopted to any frameworks. To be robust to the number of key-points detected, we propose a sparse encoding method to ensure that each key-point can only affect a small part of the object descriptors, making the global descriptors robust in severe conditions such as viewpoint changes and object deformation. In the experiments, we show that it achieves superior performance in object matching and provides reliable semantic relocalization. We also show a live demo to demonstrate its robustness. We expect that this method will play an important role in robotic applications.

## REFERENCES

- [1] C. Wang, W. Wang, Y. Qiu, Y. Hu, and S. Scherer, "Visual memorability for robotic interestingness via unsupervised online learning," in *European Conference on Computer Vision (ECCV)*, 2020.
- [2] H. Wang, C. Wang, and L. Xie, "Online visual place recognition via saliency re-identification," in *IEEE/RSJ International Conference on Intelligent Robots and Systems (IROS)*, 2020.
- [3] M.-P. Dubuisson and A. K. Jain, "A modified hausdorff distance for object matching," in *Proceedings of 12th international conference on pattern recognition*, vol. 1. IEEE, 1994, pp. 566–568.
- [4] R. Mur-Artal and J. D. Tardós, "Orb-slam2: An open-source slam system for monocular, stereo, and rgb-d cameras," *IEEE Transactions on Robotics*, vol. 33, no. 5, pp. 1255–1262, 2017.
- [5] D. DeTone, T. Malisiewicz, and A. Rabinovich, "Superpoint: Self-supervised interest point detection and description," in *Proceedings of the IEEE conference on computer vision and pattern recognition workshops*, 2018, pp. 224–236.
- [6] P.-E. Sarlin, D. DeTone, T. Malisiewicz, and A. Rabinovich, "Super-Glue: Learning feature matching with graph neural networks," in *CVPR*, 2020.
- [7] C. Wang, Y. Qiu, and S. Scherer, "Lifelong graph learning," *arXiv preprint arXiv:2009.00647*, 2020.
- [8] K. He, G. Gkioxari, P. Dollár, and R. Girshick, "Mask r-cnn," in *Proceedings of the IEEE international conference on computer vision*, 2017, pp. 2961–2969.
- [9] A. Glover, W. Maddern, M. Warren, S. Reid, M. Milford, and G. Wyeth, "Openfabmap: An open source toolbox for appearance-based loop closure detection," in *Robotics and automation (ICRA), 2012 IEEE international conference on*. IEEE, 2012, pp. 4730–4735.
- [10] H. Bay, T. Tuytelaars, and L. Van Gool, "Surf: Speeded up robust features," in *European conference on computer vision*. Springer, 2006, pp. 404–417.
- [11] D. Gálvez-López and J. D. Tardós, "Bags of binary words for fast place recognition in image sequences," *IEEE Transactions on Robotics*, vol. 28, no. 5, pp. 1188–1197, 2012.
- [12] E. Rublee, V. Rabaud, K. Konolige, and G. Bradski, "Orb: An efficient alternative to sift or surf," in *Computer Vision (ICCV), 2011 IEEE international conference on*. IEEE, 2011, pp. 2564–2571.
- [13] E. García-Fidalgo and A. Ortiz, "ibow-lcd: An appearance-based loop-closure detection approach using incremental bags of binary words," *IEEE Robotics and Automation Letters*, vol. 3, no. 4, pp. 3051–3057, 2018.
- [14] D. Schlegel and G. Grisetti, "Hbst: A hamming distance embedding binary search tree for visual place recognition," *arXiv preprint arXiv:1802.09261*, 2018.
- [15] P. L. N. Carrasco, F. Bonin-Font, and G. Oliver-Codina, "Global image signature for visual loop-closure detection," *Autonomous Robots*, vol. 40, no. 8, pp. 1403–1417, 2016.
- [16] M. Gehrig, E. Stumm, T. Hinzmann, and R. Siegwart, "Visual place recognition with probabilistic voting," in *2017 IEEE International Conference on Robotics and Automation (ICRA)*. IEEE, 2017, pp. 3192–3199.
- [17] S. Leutenegger, M. Chli, and R. Siegwart, "Brisk: Binary robust invariant scalable keypoints," in *2011 IEEE international conference on computer vision (ICCV)*. Ieee, 2011, pp. 2548–2555.
- [18] K. A. Tsintotas, L. Bampis, and A. Gasteratos, "Assigning visual words to places for loop closure detection," in *2018 IEEE International Conference on Robotics and Automation (ICRA)*. IEEE, 2018, pp. 1–7.
- [19] B. Fritzke, "A growing neural gas network learns topologies," in *Advances in neural information processing systems*, 1995, pp. 625–632.
- [20] E. Stumm, C. Mei, S. Lacroix, J. Nieto, M. Hutter, and R. Siegwart, "Robust visual place recognition with graph kernels," in *Proceedings of the IEEE Conference on Computer Vision and Pattern Recognition*, 2016, pp. 4535–4544.
- [21] D. Schlegel and G. Grisetti, "Adding cues to binary feature descriptors for visual place recognition," in *2019 International Conference on Robotics and Automation (ICRA)*. IEEE, 2019, pp. 5488–5494.
- [22] C. Wang, J. Yang, L. Xie, and J. Yuan, "Kervolutional neural networks," in *The IEEE Conference on Computer Vision and Pattern Recognition (CVPR)*, 2019, pp. 31–40.
- [23] Z. Chen, A. Jacobson, N. Sünderhauf, B. Upcroft, L. Liu, C. Shen, I. Reid, and M. Milford, "Deep learning features at scale for visual place recognition," in *2017 IEEE International Conference on Robotics and Automation (ICRA)*. IEEE, 2017, pp. 3223–3230.
- [24] R. Arandjelovic, P. Gronat, A. Torii, T. Pajdla, and J. Sivic, "Netvlad: Cnn architecture for weakly supervised place recognition," in *Proceedings of the IEEE conference on computer vision and pattern recognition*, 2016, pp. 5297–5307.
- [25] S. Hausler, A. Jacobson, and M. Milford, "Multi-process fusion: Visual place recognition using multiple image processing methods," *IEEE Robotics and Automation Letters*, vol. 4, no. 2, pp. 1924–1931, 2019.
- [26] N. Dalal and B. Triggs, "Histograms of oriented gradients for human detection," in *Proceedings of the IEEE Computer Society Conference on Computer Vision and Pattern Recognition (CVPR)*, 2005.
- [27] H. F. Zaki, F. Shafait, and A. Mian, "Convolutional hypercube pyramid for accurate rgb-d object category and instance recognition," in *2016 IEEE International Conference on Robotics and Automation (ICRA)*. IEEE, 2016, pp. 1685–1692.
- [28] M. Schwarz, H. Schulz, and S. Behnke, "Rgb-d object recognition and pose estimation based on pre-trained convolutional neural network features," in *2015 IEEE international conference on robotics and automation (ICRA)*. IEEE, 2015, pp. 1329–1335.
- [29] H. F. Zaki, F. Shafait, and A. Mian, "Viewpoint invariant semantic object and scene categorization with rgb-d sensors," *Autonomous Robots*, vol. 43, no. 4, pp. 1005–1022, 2019.
- [30] D. G. Lowe, "Distinctive image features from scale-invariant keypoints," *International journal of computer vision*, vol. 60, no. 2, pp. 91–110, 2004.
- [31] P. Veličković, G. Cucurull, A. Casanova, A. Romero, P. Liò, and Y. Bengio, "Graph Attention Networks," *International Conference on Learning Representations (ICLR)*, 2018.
- [32] K. Simonyan and A. Zisserman, "Very deep convolutional networks for large-scale image recognition," *arXiv:1409.1556*, 2014.
- [33] M. J. Tarr and W. G. Hayward, "The concurrent encoding of viewpoint-invariant and viewpoint-dependent information in visual object recognition," *Visual Cognition*, vol. 25, no. 1-3, pp. 100–121, 2017.
- [34] H. Lee, A. Battle, R. Raina, and A. Y. Ng, "Efficient sparse coding algorithms," in *Advances in neural information processing systems*. Citeseer, 2007, pp. 801–808.
- [35] Y. Gwon, M. Cha, and H. Kung, "Deep sparse-coded network (dsn)," in *2016 23rd International Conference on Pattern Recognition (ICPR)*. IEEE, 2016, pp. 2610–2615.
- [36] X. Liu, W. Li, J. Huo, L. Yao, and Y. Gao, "Layerwise sparse coding for pruned deep neural networks with extreme compression ratio," in *Proceedings of the AAAI Conference on Artificial Intelligence*, vol. 34, no. 04, 2020, pp. 4900–4907.
- [37] T.-Y. Lin, M. Maire, S. Belongie, J. Hays, P. Perona, D. Ramanan, P. Dollár, and C. L. Zitnick, "Microsoft coco: Common objects in context," in *European conference on computer vision*. Springer, 2014, pp. 740–755.
- [38] G. Hinton, N. Srivastava, and K. Swersky, "Neural networks for machine learning lecture 6a overview of mini-batch gradient descent," *Cited on*, vol. 14, no. 8, 2012.
- [39] P.-E. Sarlin, C. Cadena, R. Siegwart, and M. Dymczyk, "From coarse to fine: Robust hierarchical localization at large scale," in *Proceedings of the IEEE/CVF Conference on Computer Vision and Pattern Recognition*, 2019, pp. 12716–12725.
- [40] Z. Liu, S. Zhou, C. Suo, P. Yin, W. Chen, H. Wang, H. Li, and Y.-H. Liu, "Lpd-net: 3d point cloud learning for large-scale place recognition and environment analysis," in *Proceedings of the IEEE/CVF International Conference on Computer Vision (ICCV)*, October 2019.
- [41] Y. Wu, J. Lim, and M.-H. Yang, "Online object tracking: A benchmark," in *IEEE Conference on Computer Vision and Pattern Recognition (CVPR)*, 2013.
- [42] M. Kristan, J. Matas, A. Leonardis, T. Vojir, R. Pflugfelder, G. Fernandez, G. Nebel, F. Porikli, and L. Čehovin, "A novel performance evaluation methodology for single-target trackers," *IEEE Transactions on Pattern Analysis and Machine Intelligence*, vol. 38, no. 11, pp. 2137–2155, Nov 2016.
- [43] J. Luiten, A. Osep, P. Dendorfer, P. Torr, A. Geiger, L. Leal-Taixe, and B. Leibe, "Hota: A higher order metric for evaluating multi-object tracking," *International Journal of Computer Vision (IJCV)*, 2020.
- [44] C. Wang, L. Zhang, L. Xie, and J. Yuan, "Kernel cross-correlator," in *Thirty-Second AAAI Conference on Artificial Intelligence (AAAI)*, 2018, pp. 4179–4186.
- [45] A. Geiger, P. Lenz, and R. Urtasun, "Are we ready for autonomous driving? the kitti vision benchmark suite," in *Conference on Computer Vision and Pattern Recognition (CVPR)*, 2012.